

## Two-flavor staggered fermion thermodynamics at $N_f=12$

Claude Bernard

*Department of Physics, Washington University, St. Louis, Missouri 63130*

Tom Blum

*Brookhaven National Laboratory, Upton, New York 11973-5000*

Carleton DeTar

*Department of Physics, University of Utah, Salt Lake City, Utah 84112*

Steven Gottlieb and Kari Rummukainen

*Indiana University, Bloomington, Indiana 47405*

Urs M. Heller

*SCRI, The Florida State University, Tallahassee, Florida 32306-4052*

James Hetrick and Douglas Toussaint

*Department of Physics, University of Arizona, Tucson, Arizona 85721*

Robert L. Sugar

*Department of Physics, University of California, Santa Barbara, California 93106*

(Received 23 May 1996)

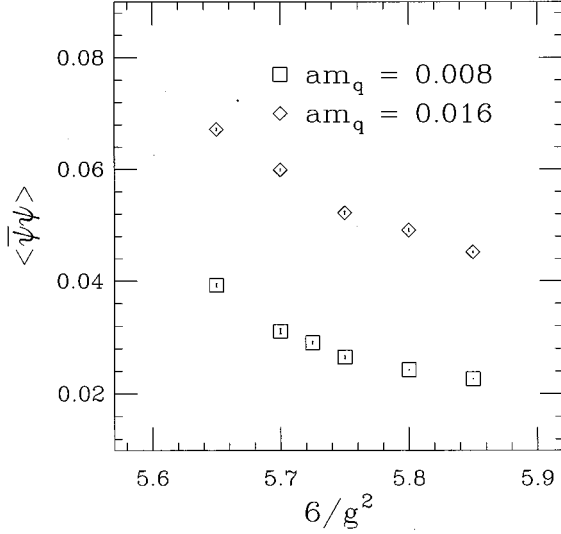
We present results of an ongoing study of the nature of the high temperature crossover in QCD with two light fermion flavors. These results are obtained with the conventional staggered fermion action at the smallest lattice spacing to date, approximately 0.1 fm. Of particular interest are (1) a study of the temperature of the crossover, an important indicator of continuum scaling, (2) a determination of the induced baryon charge and baryon susceptibility, used to study the dissolution of hadrons at the crossover, (3) the scalar susceptibility, a signal for the appearance of soft modes, and (4) the chiral order parameter, used to test models of critical behavior associated with chiral symmetry restoration. From our new data and published results for  $N_f=4$ , 6, and 8, we determine the QCD magnetic equation of state from the chiral order parameter using  $O(4)$  and mean field critical exponents and compare it with the corresponding equation of state obtained from an  $O(4)$  spin model and mean field theory. We also present a scaling analysis of the Polyakov loop, suggesting a temperature-dependent “constituent quark free energy.” [S0556-2821(96)01619-0]

PACS number(s): 12.38.Gc, 11.15.Ha, 12.38.Aw, 12.38.Mh

### I. INTRODUCTION

Lattice simulations of high temperature QCD provide, at present, our only firmly grounded theoretical insights into the phenomenology of the transition from hadronic matter to the quark-gluon plasma, and into the nature of the plasma itself. Our ultimate goals in lattice simulations at high temperature include (1) establishing continuum scaling, important not only for determining the temperature of the crossover, but necessary for the validity of all dynamical fermion simulations, (2) establishing the mechanism for the dissolution or formation of hadrons at the crossover, (3) exploring the intricate critical behavior associated with the phase transition, and (4) obtaining a quantitative characterization of the quark-gluon plasma, including the equation of state. To achieve these goals requires a combination of advances in algorithms and computing power [1,2]. Recent improvements in quenched lattice algorithms hold promise for dynamical fermion simulations [3,4]. Here we present results of simulations with the conventional staggered fermion action at the smallest lattice spacing to date.

The most detailed previous simulations with two flavors of staggered fermions were carried out at  $N_f=4$  ( $a \approx 0.3$  fm) [5],  $N_f=6$  ( $a \approx 0.2$  fm) [6], and  $N_f=8$  ( $a \approx 0.15$  fm) [7]. Results of those simulations reaffirmed the hypothesis that for two flavors there is a rapid crossover, but no phase transition at nonzero quark mass. Moreover, the ratio  $T_c/m_\rho$  was found to be consistent with previous measurements. Despite the lack of surprises at  $N_f=6$  and 8, there are strong reasons to push to still smaller lattice spacing. The full flavor symmetry in the staggered fermion scheme is restored only in the continuum limit.  $\sigma$  models of chiral symmetry restoration suggest that the crossover becomes a first order phase transition as the number of flavors is increased [8]. If flavor symmetry breaking were to cause an effective undercounting of quark flavors, one might expect a more pronounced crossover, or even a genuine phase transition at smaller lattice spacing. Moreover, strong coupling distortions in the hadron spectrum at  $N_f=6$  undermine credibility in a determination of the crossover temperature or even in the plausibility of having achieved a scaling ratio  $T_c/m_\rho$ . For these reasons we undertook a simulation at  $a \approx 0.1$  fm. Preliminary results

FIG. 1. Chiral condensate  $\langle \bar{\psi}\psi \rangle$  vs  $6/g^2$ .

were reported at the Bielefeld and Melbourne Lattice conferences [2,9,10].

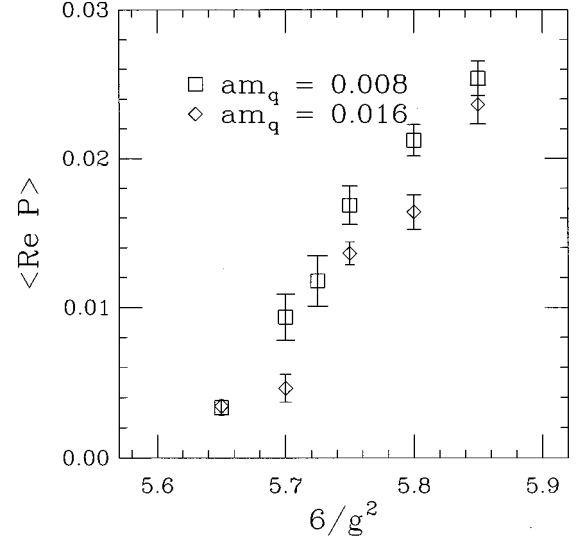
The simulation with two flavors was carried out using the R algorithm described in [11] at two quark masses,  $am_q = 0.008$  and  $0.016$  and six couplings,  $6/g^2 = 5.65, 5.70, 5.725, 5.75, 5.80, 5.85$ , except that the  $5.725$  coupling was not simulated at the higher mass. In each case the simulation was extended to at least 2000 molecular dynamics time units. Lattices were saved at intervals of eight time units. For the present analysis the first 500 time units were omitted for equilibration. Most of the results reported here are based on an analysis of approximately 180 remaining lattices at each parameter pair. For the sake of comparison, we also present some new results for  $N_t = 6$ , based on a compilation of lattices from our equation of state study [12].

In addition to the standard variables, the chiral order parameter and the Polyakov loop, we introduce a fuzzy Polyakov loop in an effort to regulate the ultraviolet divergence that becomes increasingly troublesome at small lattice spacing. We also measure the baryon susceptibility, the induced quark number, and the disconnected chiral susceptibility. Results are presented in Sec. II. We show that with our choice of masses and couplings, the crossover is more clearly defined in terms of the baryon susceptibility and induced quark number. In Sec. III we present a scaling analysis of the Polyakov loop variable for world data ranging from  $N_t = 4$  to  $N_t = 12$ , in terms of a constituent quark free energy. We also present a critical scaling analysis of the dependence of  $\langle \bar{\psi}\psi \rangle$  on temperature and quark mass (magnetic equation of state), including a compilation of world data for this variable. This analysis is carried out in the context of mean field as well as  $O(4)$  critical behavior.

## II. LOCATING THE CROSSOVER

### A. Polyakov loop, $\langle \bar{\psi}\psi \rangle$ , fuzzy loop

The high temperature crossover is conventionally located from the inflection point in a plot of the Polyakov loop or chiral order parameter as a function of coupling. Figures 1

FIG. 2. Polyakov loop vs  $6/g^2$ .

and 2 plot these quantities at fixed bare quark mass as a function of coupling. It is clear that despite the small errors, at these quark masses the effect of the crossover on these quantities is subtle, indeed.

The Polyakov loop measures the change  $f(T, m_q)$  in the ensemble free energy caused by the introduction of a static test quark. In particular, with our normalization

$$\langle \text{Re } P \rangle = 3 \exp[-f(T, m_q)/T]. \quad (2.1)$$

As the lattice spacing shrinks, the test quark self-energy develops an ultraviolet divergence, which may overwhelm a crossover signal in this quantity. Thus one might hope that by increasing the radius of the test charge, one might regulate the divergence and recover a signal at least as strong as was seen on a coarser lattice. Accordingly, we constructed a “fuzzy Polyakov loop” variable in analogy with techniques introduced for glueball sources [14]. To do so, we replaced the conventional product of forward links,

$$\langle \text{Re } P(\mathbf{x}) \rangle = \left\langle \text{Tr} \prod_{t=0}^{N_t-1} U_t(\mathbf{x}, t) \right\rangle, \quad (2.2)$$

with

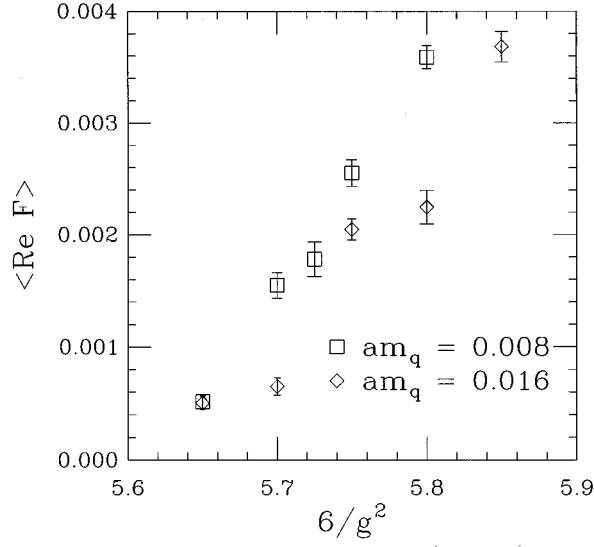
$$\langle \text{Re } F(\mathbf{x}) \rangle = \left\langle \text{Tr} \prod_{t=0}^{N_t-1} F_t(\mathbf{x}, t) \right\rangle, \quad (2.3)$$

where

$$F_t(\mathbf{x}, t) = \alpha U_t + \beta \sum U_{\text{staple}}. \quad (2.4)$$

The six staples associated with the link  $U_t(\mathbf{x}, t)$  are the usual three-link products of the form

$$U_x(\mathbf{x}, t) U_t(\mathbf{x} + \hat{x}, t) U_x^\dagger(\mathbf{x}, t+1) \quad (2.5)$$

FIG. 3. Fuzzy Polyakov loop vs  $6/g^2$ .

centered on the link from  $(\mathbf{x}, t)$  to  $(\mathbf{x}, t+1)$ . A weighting  $\alpha = \beta = 1/7$  was determined from a rough optimization of the variance. By construction the weights sum to 1 and we do not project the matrix  $F_i$  onto  $SU(3)$ , so this observable still creates a source of precisely one color triplet.

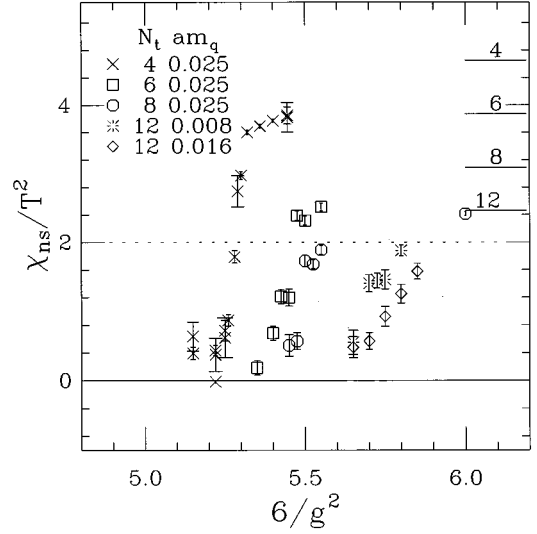
Figure 3 gives the result. Comparing with the standard Polyakov loop in Fig. 2, we see that smearing indeed reduces the relative statistical error, but apparently does not enhance the crossover signal.

### B. Baryon susceptibility

The conventional Feynman path integral simulates the grand canonical ensemble in baryon number at zero chemical potential. The baryon susceptibility measures fluctuations in the baryon number of the ensemble. It is defined as the derivative of the baryon charge density with respect to chemical potential. The susceptibility can be defined separately for each flavor. Thus with two quark flavors, two susceptibilities can be measured: a flavor singlet and flavor nonsinglet [15]. Both quantities are obtained at zero chemical potential.

$$\chi_{s,ns} = \left( \frac{\partial}{\partial \mu_u} \pm \frac{\partial}{\partial \mu_d} \right) (\rho_u \pm \rho_d). \quad (2.6)$$

The nonsinglet susceptibility is compared with results for lower  $N_t$  [15] in Fig. 4. Also indicated is the free lattice quark value for each  $N_t$ . A common feature is the abrupt rise in susceptibility at crossover, followed by an asymptotic approach to the free lattice quark value. At lower values of  $N_t$ , where the crossover has been located with traditional methods, we find that the baryon susceptibility reaches 1/3–1/2 of the free quark asymptotic value at the crossover. Since this observable is based on a conserved charge, it is not renormalized, and offers our most distinctive signal for the crossover. Following the same rule for  $N_t=12$  places the crossover in the  $am_q=0.008$  series between  $6/g^2=5.65$  and  $5.70$  and in the  $am_q=0.016$  series between  $6/g^2=5.75$  and  $5.80$ .

FIG. 4. Nonsinglet baryon susceptibility vs  $6/g^2$  for  $N_t=4,6,8,12$ . Free lattice quark values for each  $N_t$  are indicated by horizontal lines on the right of the plot.

To convert these results to a temperature, we use a scale in which the  $\rho$  meson mass is taken to be 770 MeV, regardless of quark mass. The  $\rho$  mass in lattice units is obtained in turn from an empirical fit to masses in a compilation of two-flavor staggered fermion spectral simulations [16], and includes an extrapolation beyond the parameter range of spectral measurements ( $6/g^2 > 5.7$ ) using tadpole-improved asymptotic scaling. Details are given in the Appendix. From the baryon susceptibility we then place the crossover at  $T_c = 143\text{--}154$  MeV $_\rho$  at the lighter quark mass and  $T_c = 142\text{--}150$  MeV $_\rho$  at the heavier quark mass.

### C. Induced quark number

Another confinement-sensitive observable is the induced quark number [17]. This observable measures the total residual light-quark number in an ensemble containing a single test quark:

$$Q_{\text{ind}} = \int \rho_{\text{ind}}(r) d^3r. \quad (2.7)$$

The induced quark number density  $\rho_{\text{ind}}$  is measured in the presence of the test quark. Operationally, the quantity measures the correlation between the Polyakov loop and the light-quark density [17].

This observable is subject to considerable fluctuation. We found it particularly effective to introduce the test charge through the fuzzy Polyakov loop variable described above. The baryon density of the dynamical quark is computed using a random source estimator [17]. To improve the signal further, we adjusted the number of random sources using an adaptive procedure on a configuration-by-configuration basis as follows: starting with a minimum of 20 random sources the variance of the total induced baryon number was estimated. If the variance was greater than tolerance, another 20 random sources were added to the sample, and so on, up to a maximum of 80 for one configuration.

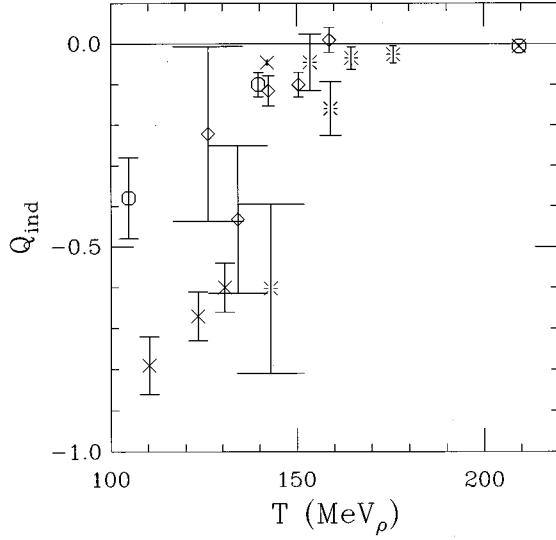


FIG. 5. Induced quark number. Crosses for  $N_t=4$  at  $am_q=0.025$ , octagons for  $N_t=4, 6$ , and  $8$  at  $am_q=0.025$  with fixed  $6/g^2$  (i.e., fixed lattice spacing), bursts for  $N_t=12$  at  $am_q=0.008$ , and diamonds for  $N_t=12$  at  $am_q=0.016$ .

Results are shown in Fig. 5 and compared with the results from simulations at lower  $N_t$ . The induced quark number is expected to be exactly  $-1$  at zero temperature, since confinement requires screening of the test charge by a single antiquark. At the crossover, this quantity rises rapidly, approaching zero in the high temperature phase. At lower  $N_t$  the induced quark number reaches approximately  $-0.1$  at crossover. Thus the induced quark number density can give an operational definition of the crossover. Applying this rule to the  $N_t=12$  data gives  $6/g^2=5.65-5.70$  ( $T=143-154$   $\text{MeV}_\rho$ ) in the  $am_q=0.008$  series and  $6/g^2=5.70-5.80$  ( $T=134-150$   $\text{MeV}_\rho$ ) in the  $am_q=0.016$  series. This crossover location is consistent with, but somewhat less precise than, that found from the baryon susceptibility.

#### D. Chiral susceptibility

Another signal for the crossover is the singlet chiral susceptibility

$$\chi_m = \left. \frac{\partial \langle \bar{\psi}\psi \rangle}{\partial m} \right|_{6/g^2}, \quad (2.8)$$

which measures fluctuations in the chiral order parameter  $\langle \bar{\psi}\psi \rangle$  [5]. Here, we differentiate with respect to equated up- and down-quark masses. Since the derivative is the space-time integral of the correlator  $\langle \bar{\psi}\psi(r) \bar{\psi}\psi(0) \rangle$ , a peak in this observable occurs at a minimum in the  $\sigma$ -meson screening mass, indicating the presence of a soft mode. Such soft modes are expected in models of critical behavior [8]. Like the  $\sigma$ -meson propagator, the singlet chiral susceptibility can be decomposed into two contributions, quark-line connected and quark-line disconnected:

$$\chi_m = \chi_{\text{conn}} + \chi_{\text{disc}}. \quad (2.9)$$

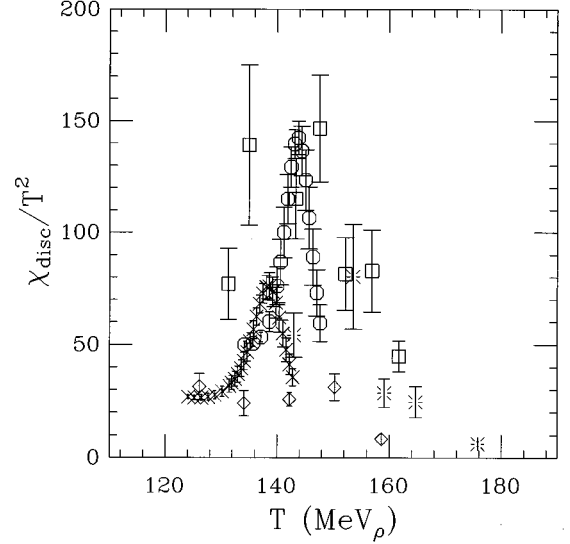


FIG. 6. Disconnected chiral susceptibility. Crosses for  $N_t=4$ ,  $am_q=0.0375$  [5], octagons for  $N_t=4$ ,  $am_q=0.02$  [5], squares for  $N_t=6$ ,  $am_q=0.0125$ , diamonds for  $N_t=12$ ,  $am_q=0.016$ , and bursts for  $N_t=12$ ,  $am_q=0.008$ .

The connected susceptibility in another guise is the derivative of  $\langle \bar{\psi}\psi \rangle$  with respect to valence quark mass at fixed sea quark mass and  $6/g^2$  [18], while the disconnected susceptibility is the configuration variance of  $\langle \bar{\psi}\psi \rangle$ :

$$\chi_{\text{disc}} = \langle \langle \bar{\psi}\psi \rangle_{\text{conf}}^2 \rangle_U - \langle \langle \bar{\psi}\psi \rangle_{\text{conf}} \rangle_U^2, \quad (2.10)$$

where  $\langle \bar{\psi}\psi \rangle_{\text{conf}}$  is the expectation value computed on a single gauge configuration and  $\langle \rangle_U$  denotes averaging over all gauge configurations in the sample.

We used the standard Gaussian random source estimator for  $\langle \bar{\psi}\psi \rangle_{\text{conf}}$ :

$$\langle \bar{\psi}\psi \rangle_{\text{conf}} = \langle \xi^\dagger S^{-1} \xi \rangle_\xi. \quad (2.11)$$

One must take care in using this estimator for Eq. (2.10), since the square involves correlated quartic terms in the random source variable. Averaging then reintroduces part of the connected susceptibility along with the disconnected susceptibility. We chose to avoid the problem altogether by computing the estimator from five separate random sources on each configuration and forming products in Eq. (2.10) only from pairs of estimators with different random sources. (For the smaller volume  $N_t=6$  data we used 33 random sources per configuration.)

Results for  $\chi_{\text{disc}}$  and  $\chi_{\text{conn}}$  are compared in Figs. 6 and 7 with the results of Karsch and Laermann at  $N_t=4$  [5] and results from a reanalysis of a set of  $N_t=6$  lattices retained from an equation of state study [12]. The benefits of the larger sample in the  $N_t=4$  data are clearly evident in this variable. At the lighter quark mass ( $am_q/T=0.08$ ) the  $N_t=4$  octagons define a crossover peak at about 145  $\text{MeV}_\rho$ . This peak can be sought in the  $N_t=6$  data at a comparable quark mass ( $am_q/T=0.075$ ). The data are crude but not inconsistent with a comparable peak. The bursts plot

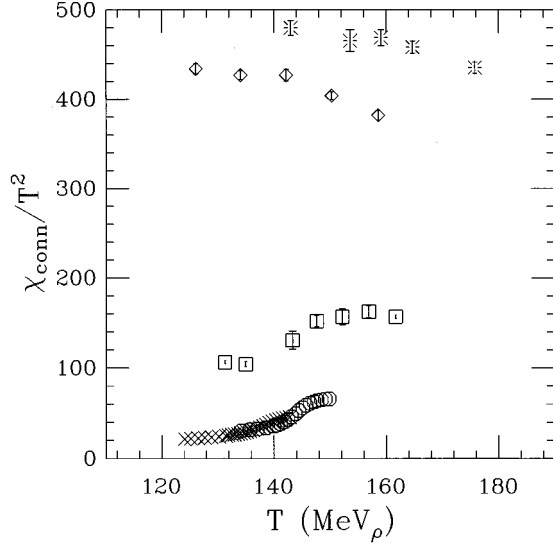


FIG. 7. Connected chiral susceptibility. Same notation as in Fig. 6.

$N_t=12$  data at the lighter quark mass ( $am_q/T=0.096$ ), which are not inconsistent with a peak in the range 140–160  $\text{MeV}_\rho$ . The signal in the higher mass  $N_t=12$  data (diamonds) is inconclusive.

That the signal in  $\chi_{\text{disc}}$  should be weaker at higher quark mass is expected from models of critical behavior that place the critical point at zero quark mass. The mass ratio  $m_\pi^2/m_\rho^2$  measures proximity to the critical point. In the  $N_t=4$  data, this ratio is less than 0.1 for the lighter quark mass ( $am_q=0.020$ ) data and between 0.1 and 0.2 for the  $am_q=0.0375$  data. For the  $N_t=6$  data it is also between 0.1 and 0.2. For the  $N_t=12$  data, it is between 0.2 and 0.3 for  $am_q=0.008$  and between 0.3 and 0.4 for  $am_q=0.016$ . Thus we expect a weakening of the crossover signal at the quark masses treated in our higher  $N_t$  data.

The connected part of the susceptibility  $\chi_{\text{conn}}$  is compared in Fig. 7 with results from  $N_t=4$  and our results from  $N_t=6$ . This quantity is far less noisy than the disconnected contribution. The lack of a discernible peak in the  $N_t=12$  results is presumably another consequence of the greater distance from the critical point.

### E. Crossover location

To summarize, the observables we have considered place the crossover at  $N_t=12$  in the range  $6/g^2=5.65\text{--}5.70$  at  $am_q=0.008$  and in the range  $5.75\text{--}5.80$  at  $am_q=0.016$ , which we translate to 143–154  $\text{MeV}_\rho$  and 142–150  $\text{MeV}_\rho$ , respectively. This determination is compared with results for a wide variety of two-flavor simulations with both Wilson and staggered fermions in Fig. 8 [9,13]. Here, we plot the temperature in units of the  $\rho$ -meson mass vs the ratio of the  $\pi$  to  $\rho$  mass. For the staggered fermion simulations, we use the lightest local (non-Goldstone) pion. This state is expected to be degenerate with the Goldstone pion in the continuum limit, so progress toward the origin in this ratio measures restoration of flavor as well as chiral symme-

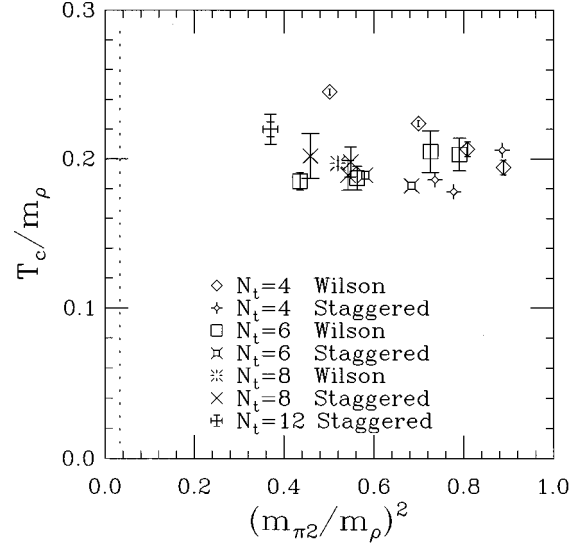


FIG. 8. Crossover temperature in units of the  $\rho$ -meson mass vs the square of the  $\pi$  to  $\rho$  mass ratio. For staggered fermions the mass of the lightest non-Goldstone pion is used [13]. The vertical line locates the physical ratio.

try. Except for a few  $N_t=4$  points from Wilson fermions, the consistency of these results (within about ten percent) is quite striking.

## III. SCALING TESTS

### A. Constituent quark free energy

The wide range of  $N_t$  values now available makes possible an amusing analysis of the Polyakov loop variable, which measures the change in the free energy of the thermal ensemble due to the introduction of a point spinless test quark. This free energy difference,

$$f(T, m_q) = -T \ln \langle \text{Re} P / 3 \rangle, \quad (3.1)$$

a function of the temperature  $T$  and light quark mass  $m_q$ , includes the lattice-regulated ultraviolet-divergent self-energy of the point source, proportional to the inverse lattice spacing  $1/a$ , and the free energy of the screening cloud of light antiquarks, quarks, and gluons, which we might call the “constituent quark free energy.” Computing the self-energy to leading order in perturbation theory, we have

$$f(T, m_q) = 2\pi C_F \alpha_V \gamma / a + f_{\text{eq}}(T, m_q), \quad (3.2)$$

where  $C_F=4/3$  is the color Casimir factor for the triplet representation,  $\alpha_V$  is the color fine structure constant appropriate for heavy quark bound states at the same lattice scale, and

$$\gamma = \frac{1}{N_s^3} \sum_k \frac{1}{6 - 2 \sum_{\mu=1}^3 \cos(2\pi k_\mu / N_s) + (Ma)^2} \quad (3.3)$$

is the dimensionless static lattice propagator for a Debye-screened electrostatic gluon field evaluated at zero separation. Screening provides an arbitrary infrared cutoff. Al-

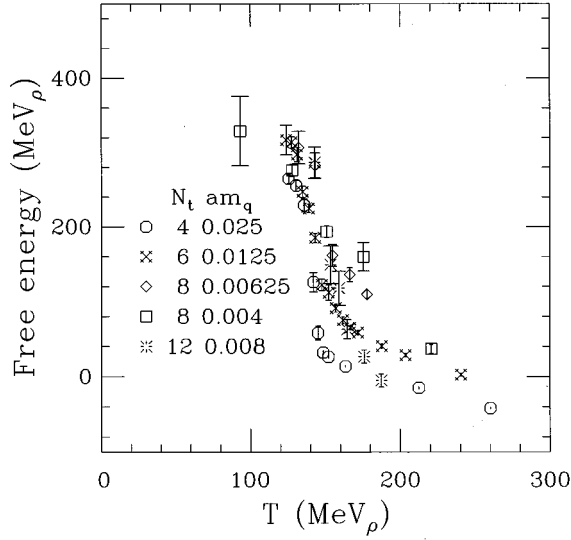


FIG. 9. Constituent quark free energy as defined in text.

though the ultraviolet divergent contribution  $1/a$  is uniquely determined in the limit  $a \rightarrow 0$ , an infrared cutoff, here embodied in the Debye mass  $M$ , determines where the contribution from the point quark ends and the contribution from the screening cloud begins. Thus this approach offers no unique definition of a “constituent quark free energy.” Instead, within the framework of any consistent definition, Eq. (3.2) permits a separation of two contributions, one varying in a known way with the lattice scale  $1/a$  and the other unknown, but scale invariant (at least in the continuum limit). Herein lies its predictive power: no matter what choice is made for the infrared cutoff, a measurement of ReP at two different values of  $N_t$  can be used to predict ReP at any other  $N_t$ .

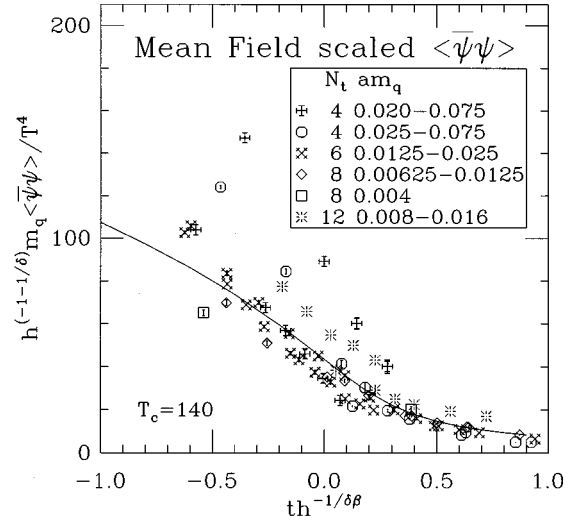
For present purposes, using  $N_t = 1/aT$ , we choose a simpler approximate form,

$$f_{cq}(T, m_q) = -T(\ln \langle \text{ReP}/3 \rangle + cN_t), \quad (3.4)$$

and adjust the dimensionless constant  $c$  by eye to achieve the rough scaling agreement shown in Fig. 9. For each data set only values for the lightest available quark mass are used. Although the quark mass values  $m_q/T$  are not the same from one  $N_t$  to the next in this figure, they are small ( $m_q/T \leq 0.1$ ) and the small variation would be expected to make little difference (of the order 10 MeV) in the free energy. The best value for  $c$  appears to be about 0.4, compared with values ranging from 0.26 to 0.35 expected from the lowest order perturbative self-energy with a screening mass  $M = 3.2T$ . It is curious that at the crossover, the free energy drops by about the 300 MeV expected in a constituent quark model with deconfinement at high temperature.

### B. Critical behavior

An  $SU(N) \times SU(N)$   $\sigma$  model has often been proposed as the paradigm for the high temperature phase transition in QCD [8]. For two light flavors ( $N=2$ ) one appealing alternative, consistent with numerical results, is that chiral symmetry restoration proceeds through a second order phase

FIG. 10. Scaled  $\langle \bar{\psi}\psi \rangle$  vs scaled temperature with mean field critical exponents at  $T_c(0) = 140$  MeV.

transition at zero quark mass with attendant  $O(4)$  critical behavior. Flavor symmetry breaking in the staggered fermion scheme preserves only an exact  $O(2)$  subgroup, so one may expect  $O(2)$  critical behavior on coarse lattices. Away from the critical point, where fluctuations are unimportant, spin systems often exhibit mean field behavior. Koćić and Kogut have even proposed that mean field behavior could extend up to the critical point, as a consequence of the composite nature of the scalar  $\sigma$  model fields as they appear in QCD [19]. While it remains to be established whether their arguments apply to QCD, we consider the mean field alternative a plausible first approximation, since we do not know the extent of the Ginzburg scaling region. Thus even if  $O(4)$  critical behavior is ultimately found in QCD at sufficiently large volume, it is possible that results imitate mean field behavior for lattices of the size considered in this study and at temperatures and quark masses that are not sufficiently close to the critical point.

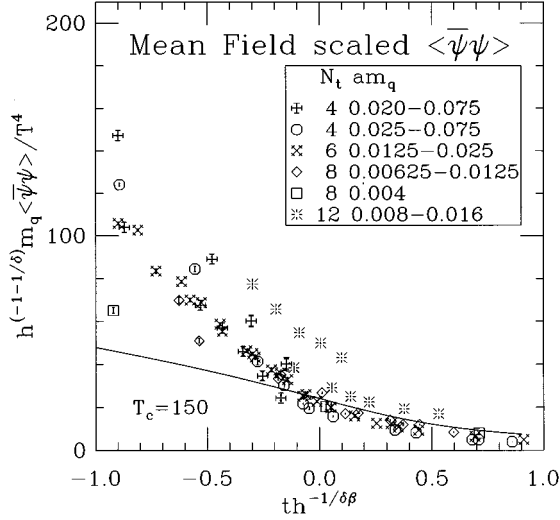
Karsch [20] and Karsch and Laermann [5] have analyzed the crossover, starting from the Fisher scaling hypothesis for the scaling of the critical contribution to the free energy

$$f_{\text{crit}}(t, h) = b^{-d} f_{\text{crit}}(b^y t, b^{y_h} h). \quad (3.5)$$

From this scaling behavior one derives a scaling relation for the critical contribution to the magnetization  $s = -\partial f_{\text{crit}}/\partial h$ :

$$s(t, h) = h^{1/\delta} y(x), \quad (3.6)$$

where  $x = th^{-1/\beta\delta}$  and  $y(x)$  is a scaling function. In QCD the quark mass plays the role of the magnetic field and  $\langle \bar{\psi}\psi \rangle$ , the magnetization. Specifically, Karsch suggests using  $h = m_q/T = am_q N_t$  and  $t = 6/g^2 - 6/g_c^2(0, N_t)$ , where  $g_c(0, N_t)$  is the critical gauge coupling at zero quark mass for a particular  $N_t$  [20]. This identification leads to a successful accounting for the crossover location (“pseudocritical point”)  $6/g_{pc}(m_q)^2$  for  $N_t = 4$  at small quark mass.

FIG. 11. Same as in Fig. 10 but with  $T_c(0)=150$  MeV.

We extend the Karsch and Laermann analysis to a wider range of lattice spacings and test the scaling relation (3.6) directly. To anticipate the need to explore critical behavior, while simultaneously approaching the continuum limit, we propose an identification that avoids quantities with anomalous dimensions, but entails a translation to physical units:

$$h = m_\pi^2(m_q, T=0) / m_\rho^2(m_q, T=0), \quad (3.7)$$

$$t = [T - T_c(0)] / T_c(0), \quad (3.8)$$

$$s = h^{-1} m_q \langle \bar{\psi}\psi(m_q, T) \rangle / T^4. \quad (3.9)$$

The scaling relation (3.6) then gives a universal function

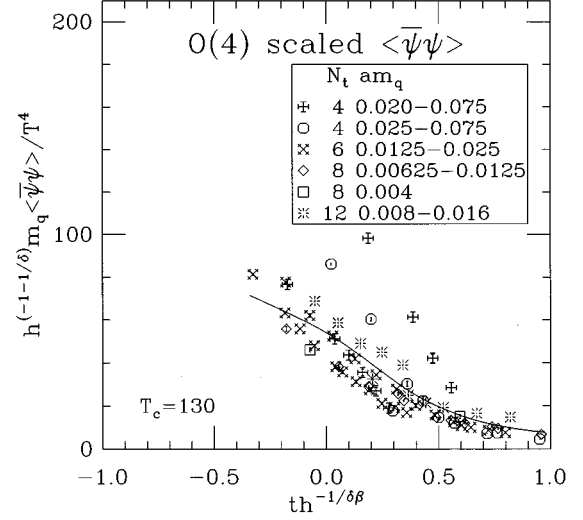
$$y(x) = h^{-1-1/\delta} m_q \langle \bar{\psi}\psi(m_q, T) \rangle / T^4 \quad (3.10)$$

with  $x = th^{-1/\delta\beta}$ . The extra factor  $h^{-1}$  is needed to compensate for the quark mass factor  $m_q$ . Let us apply this analysis to data for  $\langle \bar{\psi}\psi \rangle$  from several groups [21]. We begin by applying the following cuts to the world data:  $m_q/T = am_q N_t < 0.2$ ;  $h \leq 0.5$ ;  $-1 \leq x \leq 1$ ;  $-0.5 \leq t \leq 0.5$ . The first cut keeps parameters within the range of the spectrum interpolation. The last three are an attempt to keep values within the region dominated by the scaling part of the free energy. Since we have no *a priori* knowledge of the extent of this region, these choices are arbitrary. Indeed, the cut on  $h$  is probably too generous, as we shall see, but we have set it high initially so that all of the  $N_t=12$  data are included.

We first carry out a mean field analysis of the data. The mean field magnetic equation of state  $y(x)$  is determined from the global minimum of the usual quartic free energy:

$$F(y, x) = by^4 + axy^2 - y, \quad (3.11)$$

where  $a$  and  $b$  are adjustable scale parameters. The third adjustable parameter is the critical temperature  $T_c(0)$  at zero

FIG. 12. Same as in Fig. 10 but with O(4) critical exponents and  $T_c(0)=130$  MeV.

quark mass, which we vary in 10 MeV increments. Our exploratory strategy is to seek the best agreement between world data (after the cuts listed above) and the resulting magnetic equation of state  $y(x)$ , giving higher priority to data with higher  $N_t$ . Setting the critical exponents to their mean field values,  $\delta=1/3$  and  $\beta=1/2$ , and adjusting  $T_c(0)$  to get the best qualitative agreement according to these preferences, we get the result shown in Fig. 10 with the choice  $T_c=140$ . Since the  $N_t=4$  data appear to be outliers, it was necessary to omit them from the fit to the mean field magnetic equation of state. Apart from the  $N_t=12$  data at higher quark mass, the agreement is surprisingly good.

Our higher mass  $N_t=12$  data are strikingly inconsistent with scaling. Indeed, as we have remarked in our analysis of the disconnected susceptibility, the  $am_q=0.016$  data are taken at values of  $h$  higher than those of the rest of the sample included in the graph. Thus it is plausible that these data are taken too far from the critical region.

An alternative strategy, the one used in [2], is to emphasize agreement among world data for the full range of  $N_t$  without regard to the mean field magnetic equation of state. Our best result is shown in Fig. 11 with the choice  $T_c=150$ . The mean field curve, based on fitting only over the range  $-0.25 < x < 0.25$  clearly does not match the data as well as it did with  $T_c=140$ .

The corresponding exercise with O(4) critical exponents  $\delta=4.82$  and  $\beta=0.38$  is shown in Figs. 12 and 13. In this case the magnetic equation of state is not known in closed form. Instead, it was obtained from a simulation of an O(4) spin model [22], using critical exponents and the critical coupling reported by Kanaya and Kaya [23]. The level of agreement is comparable to that of the mean field analysis.

At the present level of precision it is not possible to distinguish O(4) from mean field critical behavior, let alone from O(2) (not shown). Obviously, a host of systematic errors, including finite volume effects and deviations from continuum scaling enter the analysis, so refinements are certainly needed before the method can serve as a definitive test of critical behavior.

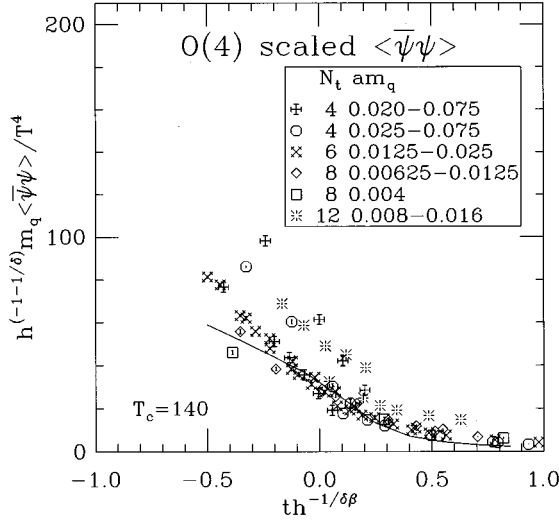


FIG. 13. Same as in Fig. 10 but with O(4) critical exponents and  $T_c(0) = 140$  MeV.

#### IV. SUMMARY AND CONCLUSIONS

We presented results of a numerical simulation of QCD with conventional staggered fermions at nonzero temperature at the smallest lattice spacing attempted to date, approximately 0.1 fm. Numerical results are collected in Tables I–IV. Most of our data is obtained in simulations at  $N_t = 12$  but some new results are also presented for  $N_t = 6$ . Locating the high temperature crossover at 0.1 fm for  $h = m_\pi^2/m_\rho^2 > 0.2$  is difficult in the conventional observables  $\langle \text{Re}P \rangle$  and  $\langle \bar{\psi}\psi \rangle$ . However, the baryon susceptibility and induced quark number show an abrupt rise consistent with what is found at lower  $N_t$ . We use these signals to locate the crossover. At the lighter quark mass it is found to be in the range 143–154 MeV  $\rho$ , consistent with results at lower  $N_t$ . Judged in terms of the ratio  $h$ , our results at higher quark mass  $am_q = 0.016$  are farther from the critical point than the world data at smaller  $N_t$ . Thus the expected crossover peak in the disconnected chiral susceptibility is barely discernible in our  $am_q = 0.016$  data set, but it is present in our  $am_q = 0.008$  data. We demonstrated a rough scaling analysis of the Polyakov loop variable in terms of a constituent quark free energy. Finally,  $\langle \bar{\psi}\psi \rangle$  shows remarkable agreement among world data with appropriate cuts over the range  $N_t = 6, 8$ , and 12 with a mean field magnetic equation of state and an assumed crossover temperature of approximately 140 MeV at zero quark mass. Our analysis is not

TABLE I. Summary of results for  $N_t = 12$ ,  $am_q = 0.008$ : chiral condensate, Polyakov loop, fuzzy Polyakov loop, and induced baryon charge.

$6/g^2$	$\langle \bar{\psi}\psi \rangle$	ReP	ReF	$Q$
5.65	0.0393(3)	0.0033(5)	0.00051(6)	−0.6(2)
5.70	0.0311(5)	0.0094(15)	0.00155(11)	−0.05(7)
5.725	0.0290(2)	0.0118(17)	0.00178(15)	−0.16(7)
5.75	0.0267(2)	0.0168(13)	0.00255(12)	−0.03(3)
5.80	0.02424(10)	0.0212(10)	0.00359(10)	−0.03(2)
5.85	0.02262(7)	0.0254(12)	—	—

TABLE II. Summary of results for  $N_t = 12$ ,  $am_q = 0.008$ : non-singlet and singlet baryon susceptibility, and disconnected and connected chiral susceptibility.

$6/g^2$	$\chi_{\text{ns}}/T^2$	$\chi_s/T^2$	$\chi_{\text{disc}}/T^2$	$\chi_{\text{conn}}/T^2$
5.65	0.6(2)	0.4(5)	54(10)	480(8)
5.70	1.40(13)	1.3(5)	80(20)	466(12)
5.725	1.44(11)	1.5(4)	29(6)	469(9)
5.75	1.52(10)	1.6(3)	25(7)	458(7)
5.80	1.87(8)	1.8(4)	6.2(1.1)	435(6)
5.85	—	—	—	—

refined enough to distinguish among O(2), O(4), and mean field scaling, however.

#### ACKNOWLEDGMENTS

We are grateful to Frithjof Karsch and Edwin Laermann for providing us with tabulations of results from their  $N_t = 4$  study. We also thank Edward Shuryak and Krishna Rajagopal for stimulating discussions. This work was supported in part by the U.S. National Science Foundation under Grants No. PHY91-16964 and PHY93-09458 and by the U.S. Department of Energy under Contracts No. DE-FG02-91ER-40661, DE2-FG02-91ER-40628, DE-FG03-95ER-40906, DE-FG05-85ER250000, and DE-FG05-92ER-40742, and was carried out through grants of computer time from the NSF at NCSA, SDSC, PSC, and by the DOE at NERSC and Sandia.

#### APPENDIX: CONVERSION FROM LATTICE TO PHYSICAL UNITS

The lattice scale is converted to physical units using  $a = am_\rho/770 \text{ MeV}^{-1}$  following a method similar to that of Ref. [16]. The numerator  $am_\rho$  is found through a combination of interpolation and extrapolation from zero temperature spectral measurements described below. Of course, taking the physical value to be 770 MeV ignores shifts in this value as the quark mass is varied. We also require masses of the Goldstone pion  $m_\pi$  and the second local pion  $m_{\pi 2}$ , which becomes degenerate with the pion in the continuum limit. Unfortunately, the highest value of  $6/g^2$  for which spectral data are available is 5.7, but our  $N_t = 12$  data span the range 5.65–5.85, requiring extrapolation. For data at lower  $N_t$  an interpolation suffices. Figure 14 indicates the parameter range of spectral data used for interpolation [24]. In selecting

TABLE III. Summary of results for  $N_t = 12$ ,  $am_q = 0.016$ : chiral condensate, Polyakov loop, fuzzy Polyakov loop, and induced baryon charge.

$6/g^2$	$\langle \bar{\psi}\psi \rangle$	ReP	ReF	$Q$
5.65	0.0672(2)	0.0034(4)	0.00050(5)	−0.2(2)
5.70	0.0599(2)	0.0046(9)	0.00065(8)	−0.4(2)
5.75	0.0522(3)	0.0136(8)	0.00205(9)	−0.12(4)
5.80	0.0491(3)	0.0164(12)	0.00225(15)	−0.10(3)
5.85	0.04516(14)	0.0236(13)	0.00368(14)	0.01(3)



TABLE IV. Summary of results for  $N_t=12$ ,  $am_q=0.016$ : non-singlet and singlet baryon susceptibility, and disconnected and connected chiral susceptibility.

$6/g^2$	$\chi_{ns}/T^2$	$\chi_s/T^2$	$\chi_{disc}/T^2$	$\chi_{conn}/T^2$
5.65	0.48(15)	0.9(4)	31(6)	434(6)
5.70	0.57(12)	0.4(5)	24(6)	427(5)
5.75	1.14(12)	0.4(4)	26(3)	427(7)
5.80	1.21(10)	1.3(3)	30(5)	404(4)
5.85	1.58(11)	1.2(4)	8(2)	382(5)

the world data sample, we have not attempted to correct for finite volume effects.

For the interpolation we found a polynomial or spline expansion convenient:

$$m_\pi/m_\rho = R_{\pi/\rho}(6/g^2, am_q) = (am_q)^{1/2} S_\pi(6/g^2) + am_q T_\pi(6/g^2) + (am_q)^{3/2} U_\pi(6/g^2), \quad (A1)$$

$$am_\rho = R_\rho(6/g^2, am_q) = S_\rho(6/g^2) + am_q T_\rho(6/g^2) + (am_q)^2 U_\rho(6/g^2), \quad (A2)$$

$$am_{\pi_2} = R_{\pi_2}(6/g^2, am_q) = S_{\pi_2}(6/g^2) + am_q T_{\pi_2}(6/g^2) + (am_q)^2 U_{\pi_2}(6/g^2), \quad (A3)$$

where the  $S$ ,  $T$ , and  $U$ 's are natural cubic splines with three knots,  $6/g^2=5.3, 5.5, 5.7$  selected to span the range of available spectral data.

For the  $N_t=12$  data over the range  $6/g^2=[5.65, 5.85]$ , we chose an extrapolation based on two-loop asymptotic scaling:

$$a\Lambda(6/g^2) = [8\pi^2/(3b_0g^2)]^{b_1/b_0} \exp[-8\pi^2/(b_0g^2)], \quad (A4)$$

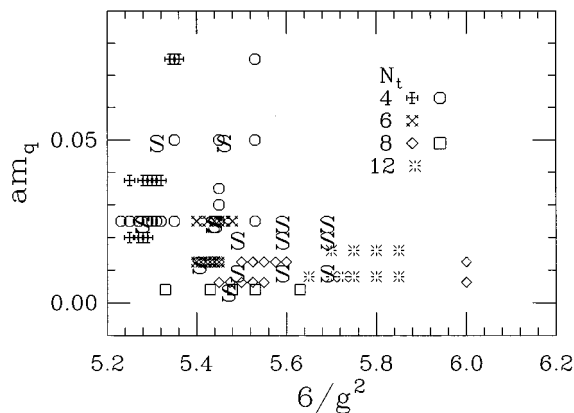


FIG. 14. Range of parameter pairs  $(6/g^2, am_q)$  for two-flavor staggered fermion thermodynamic simulations (various plot symbols as indicated) and spectral data (symbol “S”) used to set the lattice scale.

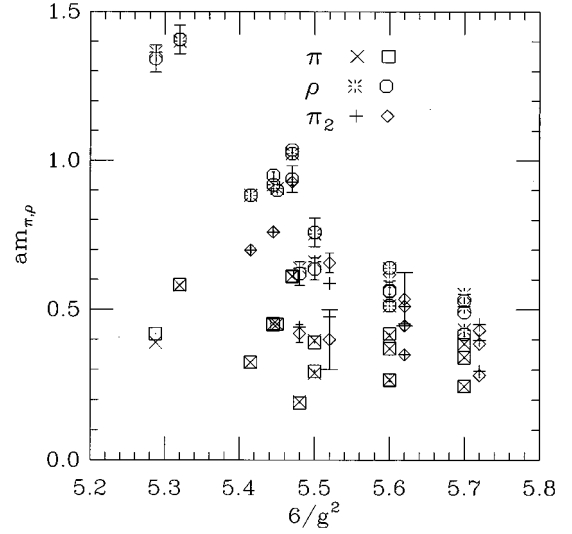


FIG. 15. Empirical fit to the  $\pi$ ,  $\rho$ , and  $\pi_2$  masses in the compilation of available spectral data. Open symbols (square, octagon, diamond) and error bars show the respective measured values. The cross, burst, and plus show the respective empirical estimates. The  $\pi_2$  values at 5.5, 5.6, and 5.7 are offset for clarity.

where  $b_0 = 11 - 2N_f/3$  and  $b_1 = 51 - 19N_f/3$  and  $N_f=2$ . In place of the bare lattice coupling, we used the tadpole-improved value proposed by Mackenzie and Lepage [3] and generalized to two flavors by Bitar *et al.* [25]:

$$6/g_{\text{eff}}^2 = \beta_{\text{eff}}(\square) = -2/\ln(\square/3) - 1.99/\pi, \quad (A5)$$

where  $\square$  is the plaquette variable (normalized to 3 for the vacuum). Applying the extrapolation requires knowledge of the plaquette over the range of extrapolation. Since zero temperature values are unavailable over this range, we used the plaquette values measured in our high temperature study, using a spline interpolation formula in the same pattern as the masses above, but with knots at  $6/g^2=5.65, 5.75, 5.85$ . At our small lattice spacing, the temperature effect on the plaquette is negligible for this purpose. To avoid introducing distortions in our predicted mass values resulting from a switch in method from the spline interpolation to the extrapolation procedure, we elected to use only an extrapolation, based on interpolated spectral data at  $6/g^2=5.65$ , the lowest value in our data set, rather than at  $6/g^2=5.70$ , the highest parameter for which spectral data is available. One must allow for a rescaling of the quark mass in the extrapolation. Thus to determine the starting point for extrapolation, we first solve for the scale parameter  $s$

$$s = \frac{\Lambda\{\beta_{\text{eff}}[\square(6/g^2, am_q)]\}}{\Lambda\{\beta_{\text{eff}}[\square(5.65, am_q/s)]\}}. \quad (A6)$$

The extrapolated masses are then obtained by rescaling from the interpolation at  $6/g^2=5.65$ :

$$m_\pi/m_\rho = R_{\pi/\rho}(5.65, am_q/s), \quad (A7)$$

$$am_p = sR_p(5.65, am_q/s), \quad (\text{A8})$$

$$am_{\pi_2} = sR_{\pi_2}(5.65, am_q/s). \quad (\text{A9})$$

The measured mass values at 5.70 can then be used as a check of the extrapolation. In Fig. 15 we compare the em-

pirical formula for hadron masses with the measured values. The extrapolation from  $6/g^2 = 5.65$  predicts slightly higher mass values at  $6/g^2 = 5.7$  than measured. The agreement is certainly adequate for present purposes. To refine the method would require a more detailed study of finite volume effects [27].

- 
- [1] Y. Iwasaki, in *Lattice '94*, Proceedings of the International Symposium, Bielefeld, Germany, edited by F. Karsch *et al.* [Nucl. Phys. B (Proc. Suppl.) **42**, 96 (1995)]; E. Laermann *et al.*, *ibid.*, p. 120.
- [2] C. DeTar, in *Lattice '94*, [1], p. 73; C. DeTar in *Quark Gluon Plasma 2*, edited by R. Hwa (World Scientific, Singapore, 1995).
- [3] G.P. Lepage and P.B. Mackenzie, in *Lattice '90*, Proceedings of the International Symposium, Tallahassee, Florida, edited by V. M. Heller, A. D. Kennedy, and A. Sanielevici [Nucl. Phys. B (Proc. Suppl.) **20**, 173 (1991)]; Phys. Rev. D **48**, 2250 (1993); P.B. Mackenzie, in *Lattice '92*, Proceedings of the International Symposium, Amsterdam, The Netherlands, edited by J. Smit and P. van Baal [Nucl. Phys. B (Proc. Suppl.) **30**, 35 (1993)].
- [4] K. Symanzik, Nucl. Phys. **B226**, 187 (1983); G. P. Lepage, in *Lattice '95*, Proceedings of the International Symposium, Melbourne, Australia, edited by T. Kiev *et al.* [Nucl. Phys. B (Proc. Suppl.) **47**, 3 (1996)]; W. Bietenholz and U.J. Wiese, in *Lattice '93*, Proceedings of the International Symposium, Dallas, Texas, edited by T. Draper *et al.*, *ibid.* **47**, 575 (1996); Nucl. Phys. **B464**, 319 (1996); T. DeGrand, A. Hasenfratz, P. Hasenfratz, and F. Niedermayer, Nucl. Phys. **B454**, 587 (1995); **B454**, 615 (1995); Phys. Lett. B **365**, 233 (1996).
- [5] F. Karsch and E. Laermann, Phys. Rev. D **50**, 6954 (1994).
- [6] C. Bernard *et al.*, Phys. Rev. D **45**, 3854 (1992).
- [7] K. Bitar *et al.*, Nucl. Phys. B (Proc. Suppl.) **30**, 316 (1993).
- [8] R. D. Pisarski and F. Wilczek, Phys. Rev. D **46**, 4657 (1992); F. Wilczek, J. Mod. Phys. A **7**, 3911 (1992); K. Rajagopal and F. Wilczek, Nucl. Phys. **B399**, 395 (1993); K. Rajagopal, in *Quark Gluon Plasma 2* [2].
- [9] MILC Collaboration, R. Sugar, in *Lattice '94* [1], p. 448.
- [10] MILC Collaboration, C. DeTar, Nucl. Phys. B (Proc. Suppl.) **47**, 499 (1996).
- [11] S. Gottlieb, W. Liu, D. Toussaint, R. L. Renken, and R. L. Sugar, Phys. Rev. D **35**, 2531 (1987).
- [12] MILC Collaboration, T. Blum, Nucl. Phys. B (Proc. Suppl.) **47**, 503 (1996); MILC Collaboration, 1996 (unpublished).
- [13]  $N_t=4$  staggered: S. Gottlieb *et al.*, Phys. Rev. Lett. **59**, 1513 (1987);  $N_t=6$  staggered: see [6];  $N_t=8$  staggered: HTMC GC Collaboration, S. Gottlieb *et al.*, Phys. Rev. D **47**, 3619 (1993); HTMC GC Collaboration, S. Gottlieb *et al.*, Nucl. Phys. B (Proc. Suppl.) **30**, 315 (1993); R. D. Mawhinney, Nucl. Phys. B (Proc. Suppl.) **30**, 331 (1993);  $N_t=4$  Wilson: K. M. Bitar *et al.*, Phys. Rev. D **43**, 2396 (1991);  $N_t=6$  Wilson: C. Bernard *et al.*, *ibid.* **46**, 4741 (1992);  $N_t=8$  Wilson: C. Bernard *et al.*, **50**, 3377 (1994).
- [14] M. Teper, Phys. Lett. B **183**, 345 (1987).
- [15] S. Gottlieb, W. Liu, R. L. Renken, R. L. Sugar, and D. Toussaint, Phys. Rev. Lett. **59**, 2247 (1987); Phys. Rev. D **38**, 2888 (1988).
- [16] T. Blum, S. Gottlieb, L. Kärkkäinen, and D. Toussaint, Phys. Rev. D **51**, 5153 (1995).
- [17] C. Bernard *et al.*, Phys. Rev. D **49**, 6051 (1994).
- [18] S. Chandrasekharan and N. Christ, Nucl. Phys. B (Proc. Suppl.) **47**, 527 (1996).
- [19] A. Koćic and J. Kogut, Phys. Rev. Lett. **74**, 3109 (1995); Nucl. Phys. **B455**, 229 (1995).
- [20] F. Karsch, Phys. Rev. D **49**, 3791 (1994).
- [21] For  $N_t=4$ : Refs. [5] and [24]; for  $N_t=6$ : Refs. [12]; for  $N_t=8$ : Refs. [13] ( $N_t=8$  staggered).
- [22] D. Toussaint (in preparation).
- [23] K. Kanaya and S. Kaya, Phys. Rev. D **51**, 2404 (1995); see also P. Butera and M. Comi, Phys. Rev. B **52**, 6185 (1995).
- [24] S. Gottlieb *et al.*, Phys. Rev. D **38**, 2245 (1988); C. Bernard *et al.*, *ibid.* **48**, 4419 (1993); M. Fukugita *et al.*, *ibid.* **47**, 4739 (1993); K. M. Bitar *et al.*, *ibid.* **49**, 6026 (1994); W. Schaffer, Nucl. Phys. B (Proc. Suppl.) **30**, 405 (1993).
- [25] K. M. Bitar *et al.*, Phys. Rev. D **48**, 370 (1993).
- [26] C. Bernard *et al.*, Phys. Rev. D **48**, 4419 (1993); S. Gottlieb *et al.*, Nucl. Phys. B (Proc. Suppl.) **34**, 366 (1994); *ibid.* **47**, 345 (1996).